Miniaturization of zoom lenses with a single moving element

Mads Demenikov[1], Ewan Findlay[2] and Andrew R. Harvey[1]

[1]School of Engineering and Physical Sciences, Heriot Watt University, Edinburgh, EH14 4AS, Scotland, UK
[2]STMicroelectronics, 33 Pinkhill, Edinburgh, EH12 7BF, Scotland, UK

Abstract: We present an analysis of single-moving-element zoom lenses in the thin-lens limit and show how the length of these zoom lenses is determined by the zoom-factor, sensor-dimension and the depth-of-focus. By decreasing the sensor size and extending the depth-of-focus, the lengths of these zoom lenses can be reduced significantly. As an example we present a ray-traced design of a miniaturized single-moving-element zoom lens with a 2.3x zoom-factor and show how the exploitation of modern miniaturized detector array combined with wavefront coding enables a reduction in length of almost three orders-of-magnitude to 10mm.

OCIS codes: (080.2740) Geometric optical design; (080.3620) Lens system design

References and links

1. K. Yamaji, "Design of zoom lenses," in *Progress in Optics*, E. Wolf, ed., (North Holland, Amsterdam, 1967), pp. 105-170 .
2. W. J. Smith, *Modern Optical Engineering*, Third edition, (McGraw-Hill, 2000).
3. J. E. R. Dowski, and W. T. Cathey, "Extended depth of field through wave-front coding," Appl. Opt. **34**, 1859-1866 (1995).
4. S. Mezouari, G. Muyo, and A. R. Harvey, "Circularly symmetric phase filters for control of primary third-order aberrations: coma and astigmatism," J. Opt. Soc. Am. A **23**, 1058-1062 (2006).
5. S. Mezouari and A. Harvey, "Phase pupil functions for reduction of defocus and spherical aberrations," Opt. Lett. **28**, 771-773 (2003).
6. S. Mezouari, G. Muyo, and A. R. Harvey, "Amplitude and phase filters for mitigation of defocus and third-order aberrations," in *Optical Design and Engineering,* 238-248 (SPIE, St. Etienne, France, 2004).
7. W. Chi and N. George, "Electronic imaging using a logarithmic asphere," Opt. Lett. **26**, 875-877 (2001).
8. D. Zalvidea and E. E. Sicre, "Phase pupil functions for focal-depth enhancement derived from a Wigner distribution function," Appl. Opt. Vol. 37, 3623-3627 (1998)
9. E. Ben-Eliezer, E. Marom, N. Konforti, and Z. Zalevsky, "Radial mask for imaging systems that exhibit high resolution and extended depths of field," Appl. Opt. **45**, 2001-2013 (2006).
10. Z. Zalevsky, A. Shemer, A. Zlotnik, E. B. Eliezer, and E. Marom, "All-optical axial super resolving imaging using a low-frequency binary-phase mask," Opt. Express **14**, 2631-2643 (2006).
11. S. Prasad, V. P. Pauca, R. J. Plemmons, T. C. Torgersen, and J. van der Gracht, "Pupil-phase optimization or extended focus, aberration corrected imaging systems," Proc. SPIE **5559**, 335–345 (2004).
12. J. Ares García, S. Bará, M. Gomez García, Z. Jaroszewicz, A. Kolodziejczyk, and K. Petelczyc, "Imaging with extended focal depth by means of the refractive light sword optical element," Opt. Express **16**, 18371-18378 (2008).
13. I. A. Prischepa, and J. E. R. Dowski, "Wavefront coded zoom lens system," in *Zoom Lenses III* 83-93, (SPIE, San Diego, CA, USA, 2001).
14. K. Kubala, E. Dowski, and W. Cathey, "Reducing complexity in computational imaging systems," Opt. Express **11**, 2102-2108 (2003).
15. G. Muyo, A. Singh, M. Andersson, D. Huckridge, and A. Harvey, "Optimized thermal imaging with a singlet and pupil plane encoding: experimental realization," in *Electro-Optical and Infrared Systems: Technology and Applications III,* 63950-63959 (SPIE, Stockholm, Sweden, 2006)..
16. G. Muyo, and A. R. Harvey, "Decomposition of the optical transfer function: wavefront coding imaging systems," Opt. Lett. **30**, 2715-2717 (2005).

1. Introduction

In designing zoom lenses, two prominent issues must be addressed: the *variator*, which is responsible for "zooming", introduces (A) defocus, and (B) variations in optical aberrations [1]. To solve problem A, most modern zoom lenses employ so-called mechanical compensation in which at least one extra moving element, a precisely controlled lens called the *compensator*, is introduced to compensate defocus introduced by the variator [2]. To solve problem B, most modern zoom lenses are designed with additional lenses which compensate for the variations in optical aberrations introduced by zooming. The complexity introduced by these traditional design approaches tends to prevent miniaturization. In this paper we show how combining extended-depth-of-focus (EDOF) techniques, such as wavefront coding (WCF) [3] or other schemes involving masks located in the aperture stop [4-12], combined with the exploitation of the small pixel-size of modern detector arrays enables miniaturization of single-moving-element (SME) zoom lenses. To our knowledge, EDOF techniques have not previously been employed in SME zoom lenses for this purpose.

Prischepa and Dowski [13] have reported a mechanically compensated zoom lens that employed WFC to solve problem B and enable a simplified and more compact mechanically compensated zoom lens with two moving single aspherical lenses. Similar simplification where aberration-correcting lens elements have been replaced with WFC has been demonstrated with infrared imaging systems [14-15] and radially symmetric phase filters have been proposed to mitigate defocus and third-order aberrations [4-6]. We show here a new solution to problem A that enables the design of ultra-compact SME zoom lenses: we replace the compensator in a conventional mechanically-compensated zoom lens with an EDOF technique so as to enable zooming with a single moving element and reduce the need for precision mechanical motion within the lens. In particular, we consider the implementation of EDOF using WFC such as is described in [3].

In section 2, we present a new analysis of SME zoom lenses from which we show that their length is limited by zoom-factor, sensor size and depth-of-focus (DOF). As a result of this we propose to miniaturize SME lenses in two steps: first by exploiting reduced sensor size and secondly by using WFC to increase the DOF. In section 3, by way of example, we describe miniaturization of a 2.3x optical SME zoom lens.

2. Analysis of SME zoom lenses

In this section we employ the paraxial approximation to obtain expressions for the overall length of a SME lens which show lucidly how the length can be reduced. These also enable a first-order design to be approximated subsequent to more rigorous design using ray-tracing. Variation of lens power can be achieved by changing the separation between two lens elements A and B according to the well-known equation $\phi_{AB} = \phi_A + \phi_B - d\phi_A\phi_B$, where ϕ_A and ϕ_B are the powers of the two lens elements and d is the displacement between lenses A and B [2]. The back-focal-length (BFL) of the combined lens system is [2]

$$BFL_{AB}(d) = (1 - \phi_A d)/\phi_{AB} \tag{1}$$

An asymmetric two-lens system suffers from a rapid variation in optical aberrations during zooming. This effect is reduced for symmetrical zoom lenses as shown in Fig. 1. These employ two fixed lenses, A and C and a moving lens B which executes the zooming function.

The zoom factor of a zoom lens is the ratio between the maximum and minimum effective focal lengths, $Z=f_{max}/f_{min}$. We define M as the ratio of the effective focal lengths of the zoom lens when lenses A and B are in contact to when lenses B and C are in contact. The powers of lenses A and B may then be written in the forms [1,2]:

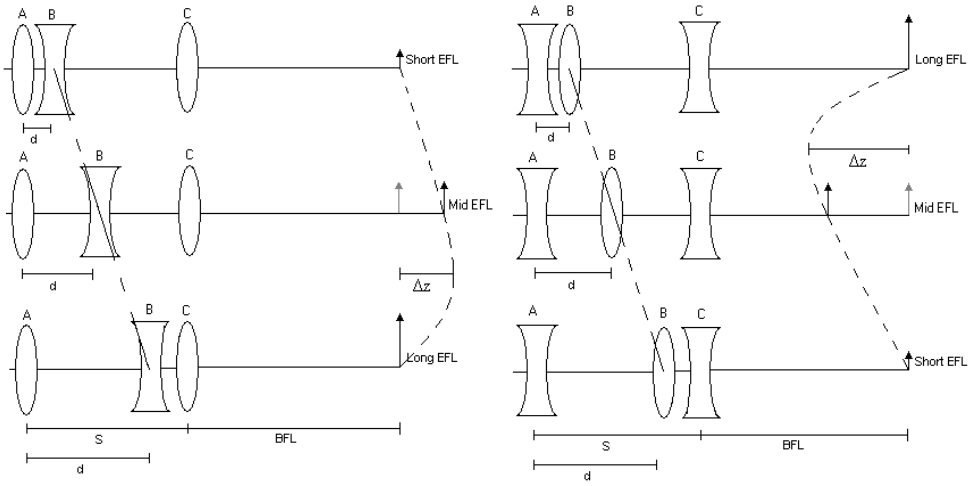

Fig. 1. Two zoom lens configurations with one moving element and a total of 3 elements showing the defocus related to the movement of lens element B. The defocus is exaggerated to show the principle and the direction. Typically, the defocus for the two SME zoom lens configurations is not identical in magnitude as also indicated by the dashed curve.

$$\begin{aligned} \phi_A &= (R-1)/(RS) \\ \phi_B &= (1-R^2)/(RS) \end{aligned} \tag{2}$$

where $R = \sqrt{M}$ and S is the distance between lenses A and C.

Lens A and B can be in the order positive, negative (+–), or negative, positive (–+): the +– configuration has $M = Z$ and the –+ configuration has $M = 1/Z$. Defocus formed by the combination of lenses A, B and C, depends on the lens displacement d and the lens powers. The focal length of the combined lenses A and B is $f_{AB} = f_A f_B /(f_A + f_B - d)$ [2], from which the focal length of a combined system of the 3 lenses, A, B and C, can be found using a re-occurrence procedure. Denoting the focal length of the combined 3-lens system at the widest field-of-view as $f_{\min}$, the power ϕ_C can be shown, using (2), to be:

$$\phi_C = \phi_A + 1/(f_{\min}\sqrt{Z}). \tag{3}$$

It can be seen that if the effective focal length at wide field-of-view is infinity, then an afocal zoom lens is obtained. The two SME zoom lens-configurations in Fig. 1 will be denoted +–+ and –+–, which refer to the signs of the powers of the lenses for an afocal system. It should be noted however that the –+–, configuration usually has a positive lens power in the rear for a focusing system. We use here the paraxial approximation to estimate the BFL of each three-lens combination as a function of S and lens displacement d [1]. The transfer-matrix of the zoom lens is:

$$\overline{\overline{T}} = \begin{pmatrix} 1 & BFL_{ABC} \\ 0 & 1 \end{pmatrix} \begin{pmatrix} 1 & 0 \\ -\phi_C & 1 \end{pmatrix} \begin{pmatrix} 1 & S-d \\ 0 & 1 \end{pmatrix} \begin{pmatrix} 1 & 0 \\ -\phi_B & 1 \end{pmatrix} \begin{pmatrix} 1 & d \\ 0 & 1 \end{pmatrix} \begin{pmatrix} 1 & 0 \\ -\phi_A & 1 \end{pmatrix}, \tag{4}$$

Focused light rays are given by $\begin{pmatrix} y' \\ \vartheta' \end{pmatrix} = \overline{\overline{T}} \begin{pmatrix} y \\ \vartheta \end{pmatrix}$, where y and y' are the light ray-height and ϑ and ϑ' are light ray-angles. Focusing at infinity ($\vartheta = 0$, $\forall\, y$) and solving for y'=0 yields the non-trivial solution for $y \neq 0$:

$$BFL_{ABC}(d,S)=\frac{1+\varphi_B(-S+d)-\varphi_A(S-\varphi_B Sd+\varphi_B d^2)}{\varphi_B+\varphi_C-\varphi_B\varphi_C S+\varphi_B\varphi_C d-\varphi_A(-1+\varphi_B d+\varphi_C(S-\varphi_B Sd+\varphi_B d^2))} \tag{5}$$

which reduces to (1) when $\varphi_C = 0$ and $S = d$. By insertion of (2) and (3) into (5), the BFL at $d = 0$ and $d = S$ is:

$$BFL = f_{\min}\sqrt{Z} \tag{6}$$

By subtracting (6) from (5), the defocus from the image plane is obtained and this goes to zero at *d=0* and *d=S*. The maximum defocus from the image plane when focusing at infinity for the two-lens configurations is then:

$$\Delta z = -\frac{f_{\min}^2 (R-1)^3 Z}{2(f_{\min}(R-1)\sqrt{Z+(1-3R)RS})}, \tag{7}$$

where the factor of two in the divisor is introduced because we assume the detector or image plane is placed midway between the extreme locations of the planes of best focus. This is the optimal location if the F-number (*F/#*) of the zoom lens is constant during zooming. Equation (7) shows that the defocus is approximately inversely proportional to the lens separation *S* and highlights the fundamental problem in miniaturizing a SME zoom lens: the overall length of the lens can be reduced only by reducing *S* and at a cost of increased defocus, Δz. The total length of the two zoom lens configurations is $L = S + BFL \pm \Delta z$ where the ± is positive for the +–+ configuration and negative for the –+–, configuration according to the defocus indicated in Fig. 1. Since Δz is much smaller than *S* and BFL, $L \approx S + BFL$ and using (7), in the thin-lens approximation,

$$L \approx \frac{x_{sensor}\sqrt{Z}\left(16(F/\#)^2(R^3+2R-1)|W_{20}|+1/2(R-1)^3 x_{sensor}\sqrt{Z}\cdot 1/\tan(\theta/2)\right)}{32(F/\#)^2 R(3R-1)|W_{20}|\tan(\theta/2)}, \tag{8}$$

where x_{sensor} is the horizontal sensor size, θ is the full-angle field-of-view and $W_{20}=\Delta z/(8(F/\#)^2)$ is the defocus parameter. According to the Hopkins criterion, acceptable image quality requires that the defocus parameter W_{20} is less than $\lambda/6$ and in this case the second term in the major brackets in (8) dominates and so for a system with acceptable defocus we can write

$$L \approx \frac{(R-1)^3 x_{sensor}^2 Z}{64(F/\#)^2 R(3R-1)|W_{20}|\tan^2(\theta/2)}. \tag{9}$$

Combining a large sensor-size and zoom-factor with application of the Hopkins criterion can lead to zoom lenses with lengths of 10m or more which severely restricts their usefulness. This would clearly be impractical and hence all modern miniature zoom lenses are mechanically compensated. Recent technology developments have yielded an order-of-magnitude reduction in sensor size: from 43mm diagonal for traditional 35mm film to a few mm for modern pixilated detectors, and hence offer scope for a two-orders-of magnitude reduction in lengths of SME lenses. Even for modern electronic imaging systems, SME lenses are relatively large. For example the use of a 3.58mm wide detector with a modest zoom factor of *Z*=2.5, $\theta = 65^\circ$ at wide field and *F/#*=2.8, the minimum lengths of the +–+ and –+– configurations are 64 mm and 154 mm respectively. This assumes that, in accordance with

Hopkin's criterion, W_{20}=λ/6 at 550 nm. The variation of minimum lengths with zoom factor for these systems is shown in Fig. 2(a). This miniaturization of SME zoom lenses, enabled by reduced sensor size alone, gives lengths which are still impractically long for many consumer applications, such as integration into mobile telephones. It can be observed from Eq. (9) that lens length, *L*, can be further reduced by allowing an increase in W_{20} and fortunately several techniques exist to achieve EDOF whilst retaining acceptable image quality [3-12]. These involve the addition of a spatial phase modulation function in the aperture stop of the lens. Whilst this necessarily suppresses the modulation-transfer-function (MTF) in comparison to a diffraction-limited imaging system, specific phase functions have been derived that yield MTFs that, for an increased range of defocus, exhibit the twin important properties of being approximately invariant to defocus and having no nulls in the MTF. Reported phase functions fall into two main classes: those with radial symmetry and those with radial antisymmetry. The symmetric masks include phase functions which vary with, for example, the logarithm or fourth power of the radius (that is by addition of spherical aberration) [4-8] and yield images with reduced contrast but that retain image sharpness over an increased DOF. Image contrast can be restored with image processing, but image sharpness is retained even in the unrestored image. The antisymmetric masks introduce both strong phase effects and reduced amplitude in the optical transfer function (OTF) so that image restoration is essential for formation of a sharp image.

For both the symmetric and antisymmetric masks the restoration of a reduced contrast image involves a reduction in the signal-to-noise ratio (SNR) of the restored image relative to the recorded image and this is the *quid pro quo* for the increased DOF. The reduction in SNR is described as a noise-gain given by [4]:

$$\gamma = \sqrt{\frac{1}{mn}\sum_{u=0}^{m-1}\sum_{v=0}^{n-1}\left|F(u,v)\right|^2}\ , \tag{10}$$

where F is the inverse filter in the frequency domain and *m,n* are the image dimensions. Although some enhancement in DOF can be attained using any of several reported antisymmetric or symmetric masks, the optimal trade of EDOF against suppression of MTF is obtained using a mask with antisymmetry [16]. Various antisymmetric phase masks have been reported [3, 11-12], but we have chosen here to use a phase mask with a linearly separable cubic profile [3] since it is the best known and offers a trade of EDOF against SNR reduction that is at least as good as other reported masks. The profile of the cubic phase mask is of the form $z(x,y)=\alpha(x^3+y^3)$ where 2α is the peak-to-peak optical-path-difference introduced and (x,y) are normalized coordinates of the aperture stop. With a simple inverse filter, where the overall system MTF is recovered to that of a near-diffraction-limited system, $F(u,v)$ is approximately inversely proportional to α and the maximum tolerable defocus is $|W_{20}|=3\alpha(1-\nu)$ [16], where ν is the normalized spatial sampling frequency. The noise-gain is then approximately proportional to the maximum defocus for which image recovery is possible.

The additional reduction in length that is facilitated when defocus can be corrected using EDOF is illustrated by Fig. 2(b), which shows the variation in length of SME zoom lenses with W_{20} for Z=2.5 and x_{sensor}=3.58 mm as given by Eq. (8). For example reducing the maximum length of the zoom lenses; from the lengths of 64mm and 115mm required to fulfill the Hopkins criteria; to a length of 10mm that is compatible with use in mobile phone cameras results in a maximum defocus of 1.76λ and 4.21λ (λ=550 nm) for the +−+ and −+− configurations respectively. This represents a three orders-orders-of-magnitude reduction compared to the impractical 10m required for a SME zoom lens based on traditional technologies: two orders-of-magnitude reduction due to the use of modern small detector arrays and an additional order-of-magnitude due to the use of WFC to increase DOF.

A lens of these dimensions may also be attained with a mechanically compensated zoom lens; the explicit trade is that the simplification of the lens mechanics attained by a single moving element with WFC is achieved with a *quid pro quo* of degradation in the SNR of the recovered image. From the presented examples, it can be seen that the +–+ zoom lens introduces less defocus and hence enables lower levels of noise degradation than the –+– zoom lens configuration.

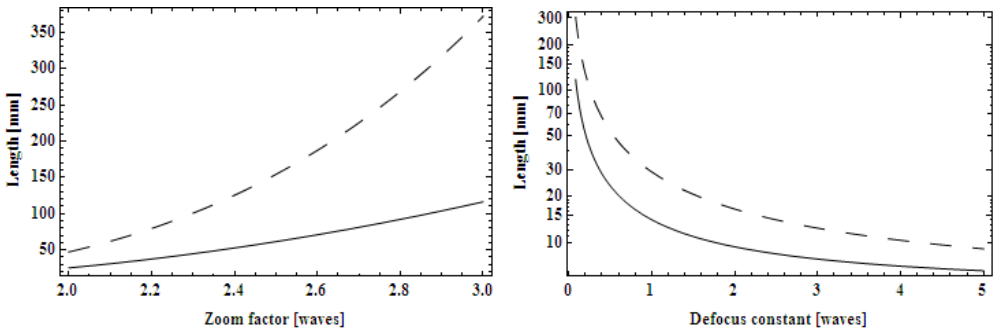

Fig. 2. Length as a function of (a) zoom factor and b) defocus constant in terms of waves for two SME zoom lens configurations. In a) defocus is given by Hopkins defocus criterion. In (b) a zoom factor of 2.5 is used. A horizontal sensor dimension of 3.58 mm is used in both cases. Solid line represents zoom lens configuration +-+ while dotted line represents zoom lens configuration -+-.

3. Design of miniaturized SME zoom lens

3.1 Location of the aperture stop and aberration control

In locating the aperture stop in the zoom systems we aim to minimize the variation in lens aberration with zooming and avoid the lens elements becoming unfeasibly thick for the curvatures required. The magnitudes of the aberrations depend on lens powers and the length of the lens and also on the configuration used. This is illustrated by the following example: for a 2.3x optical zoom lens with length of 10mm, a horizontal sensor size of 3.58mm, and field of view of $\theta = 65^{\circ}$; the minimum focal length is f_{min}=2.813mm and the travel of the moving element is restricted to 2.5 mm. These conditions dictate the focal lengths of the three groups in the zoom lens via Eqs. (2)-(3). The values for the focal lengths of the lens groups are given in Table 1 below.

Table 1. Lens focal lengths for a 2.3X optical zoom lens with lens B travelling by 2.5 mm

Configuration	EFL - Lens A	EFL - Lens B	EFL - Lens C
+-+	7.34mm	-3.92mm	2.70mm
-+-	-4.84mm	3.92mm	36.00mm

For this example the –+– configuration requires higher focal ratios for the lens groups and therefore more readily enables low levels of aberrations. Ray-tracing analysis has also indicated that low aberrations are more readily achieved in the –+– configuration. This configuration is therefore preferable although the levels of defocus, and consequently noise gain, are higher. For the –+– configurations the stop can realistically only be placed at element 2 and as is common, the system F/# will vary with zooming.

3.2 Example of a miniaturized SME zoom lens with WFC

As an example of a miniaturized design, we have used the first-order design considerations above as the basis for the design of a 2.3x SME zoom lens with WFC for alleviation of aberrations. The ray-traced optical design is shown in Fig. 3(a) and the calculated defocus with respect to obtained by subtracting (5) from (6); is shown in Fig. 3(b) together with values of defocus obtained by ray tracing at five discrete lens positions. The optimal sensor position (shown as defocus of 0mm in Fig 3b) is that which gives equal magnitude of defocus parameter at the defocus extrema at lens positions 0.9mm and 2.5mm, such that the absolute maximum defocus parameter is minimized. The small discrepancy in defocus between the paraxial approximations and the ray-trace design is generally observed and indicates that they serve as a good first-order approximation on which a detailed design may be based. The zoom lens consists of three groups: the first group is fixed and consists of a single aspheric plastic element; the second group is the variator, consisting of 2 aspheric plastic elements, the aperture stop and a spherical cemented glass doublet; the third group is fixed and consists of two aspheric plastic elements.

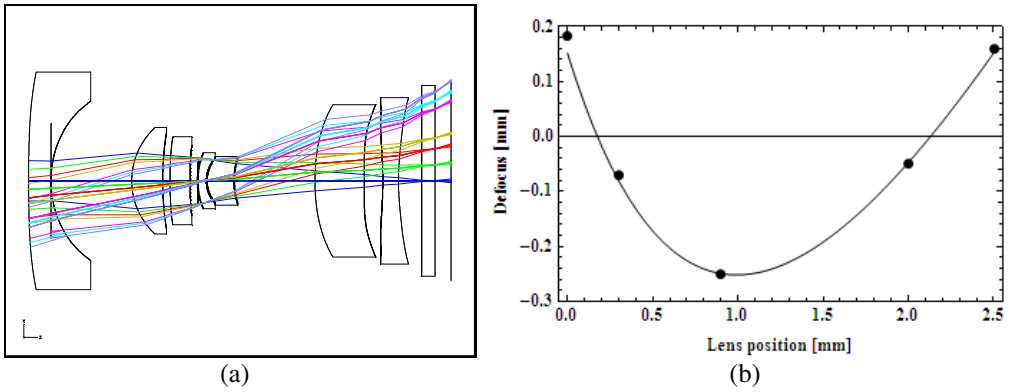

(a) (b)

Fig. 3. (a). Layout and ray-traces of the example zoom lens for lens displacement of 0.9mm and (b) the calculated defocus versus lens position with 5 defocus points obtained by ray-tracing.

The lens has been designed with a maximum aperture that varies between F/3.8 at wide field-of-view and F/6.7 for the narrow field-of-view. The defocus parameter from the optimal sensor position is W_{20}=-2.36λ (λ=550nm) at lens position 0.9mm and W_{20}=2.36λ at lens position 2.5mm (wide field of-view) and W_{20}=0.76λ at lens position 0.0mm (narrow field of view). In this article we report the mitigation of this defocus by use of cubic phase modulation at the aperture stop, although other EDOF techniques may also be used.

To obtain good radiometric sensitivity and for ease of manufacture it is common to use pixels significantly larger than the PSF and this introduces aliasing and attenuation of higher spatial frequencies by the pixel response function. A good trade-off of noise-gain against insensitivity to defocus is obtained when the phase mask is sufficiently strong to prevent excessive suppression of the MTF for all spatial frequencies below the Nyquist frequency of the imager. If the image is sampled by the detector at 50% of the optical cut-off frequency, then the maximum defocus can be mitigated with a phase mask with α=1.57λ (according to $|W_{20}|=3\alpha(1-\nu_N)$ [16]) where ν_N is the normalized Nyquist spatial-frequency. This corresponds to a peak-to-peak surface relief of 3.78 microns at 550 nm. The sampled on-axis PSFs (1.75 micron pixel size) and on-axis MTFs (up to Nyquist frequency 142 cycles/mm) with and without the phase mask are shown in Fig. 4 for zoom positions corresponding to focal lengths of 6.6mm, 4.5mm and 2.9mm. The MTFs for a conventional mechanically compensated zoom

lens with two moving elements are also included in the MTF plots for comparison. Mechanical compensation involves movement of the third lens group to retain sharp focus.

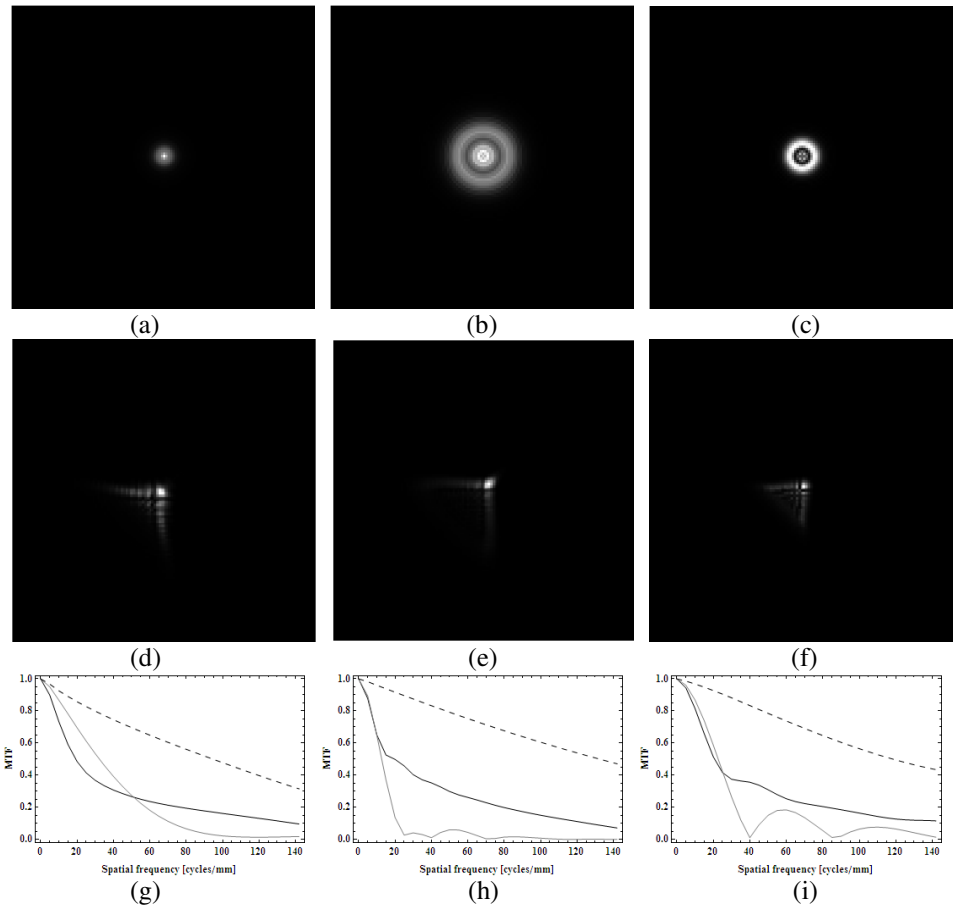

Fig. 4. PSFs without phase mask at lens position (a) 0.0 mm, (b) 0.9 mm and (c) 2.5 mm and PSFs with phase mask at lens position (d) 0.0 mm, (e) 0.9 mm and (f) 2.5 mm. Image size is 224 microns by 224 microns. MTFs with and without phase mask at lens position (g) 0.0 mm, (h) 0.9 mm and (i) 2.5 mm. Black line is the MTF in a SME zoom lens with phase mask, whilst gray line is the MTF in a SME zoom lens without phase mask. Dashed line is the in-focus MTF which could be obtained in a conventional mechanically-compensated zoom lens with two moving elements.

For the SME zoom lens without WFC, the high degree of suppression of the MTFs introduces, in general, excessive blur in the recorded image and the zeros in the MTF prevent efficient image recovery. In comparison, the use of WFC in the SME zoom lens results in some suppression of the MTF (compared to a mechanically compensated zoom lens), but the absence of zeros and the modest degree of suppression enable recovery of an image to diffraction-limited performance. Therefore, whilst the use of WFC enables enhanced image quality compared to a conventional SME zoom lens of the same length, the SNR in the recovered image will be inferior to that of a mechanically compensated zoom lens.

The PSFs for the wavefront-coded lens exhibit significant variations with zoom, as illustrated by Figs. 4(d) to 4(f), that supplement additional variations with system F/#. It is therefore necessary to select the kernel used in image recovery to be appropriate to the zoom and F/# used in image acquisition. The noise-gain introduced by WFC therefore also varies with zoom

and this combines with variations in optical throughput during zooming that are also common to conventional zoom lenses. We compare now the imaging performance of a wavefront-coded SME zoom lens with the equivalent SME zoom lens without WFC and also with the equivalent mechanically compensated zoom lens at wide field-of-view; that is at lens position of 2.5mm. We assume a relatively low, but not uncommon, detected SNR of 36dB and infinite conjugate imaging. Simulated images acquired without WFC and with mechanical compensation are shown in Figs. 5(a) and 5(b) respectively. The image recorded at the detector for the wavefront coded zoom lens is shown in Fig. 5(c) and the image obtained by recovery of this image with a Wiener filter is shown in Fig. 5(d).

Fig. 5. Images with lens position at 2.5mm acquired with (a) no implementation of phase mask, with (b) mechanically compensation, -with (c) implementation of phase mask before restoration and (d) with implementation of phase mask after restoration.

Comparison of Figs. 5(a) and 5(d) illustrates that in terms of image quality, implementing WFC in a SME zoom lens involves trading blur that varies with zoom and will generally be excessive, for good image sharpness at all zoom positions, but accompanied by a modest gain in noise level. Comparison of Figs. 5(b) with 5(d) illustrates that the enhanced simplicity of the SME zoom lens compared to a mechanically compensated lens is gained at the expense a penalty of a modest noise-gain factor of 4.82.

The principal characteristic of WFC exploited in this design technique is therefore that a high-quality image can be restored in the presence of the defocus introduced by miniaturization; that is to say, that WFC enables a degree of miniaturization of SME zoom lenses that does not appear to be possible by conventional optical design. An additional

benefit is the increase in instantaneous DOF for a given zoom position that is obtained from the relative invariance of the MTF with defocus. The most pertinent comparison for such a miniaturized zoom lens is however with the equivalent mechanically compensated lens: the use of WFC has enabled simplification of the design since only one moving element is required whereas conventional zoom lenses require two. The *quid quo pro* however is a modest decrease in the SNR of the final image.

As a final remark, it should be noted that the above calculations and simulations are based on the assumption of infinite conjugate imaging. For finite conjugate imaging some adjustment in detector positioning and α is required: the position of the detector can be adjusted such that the magnitude of the maximum negative defocus (infinite conjugate imaging, mid zoom) is equal to the magnitude of the maximum positive defocus (shortest object distance imaging, wide field-of-view). This is equivalent to focusing on the hyperfocal distance to maximize depth-of-field as is used in conventional imaging. For finite conjugate imaging with a minimum object distance of 10cm the maximum defocus parameter becomes $\pm 2.89\lambda$ at 550nm, which can be mitigated with a cubic phase mask with $\alpha=1.93\lambda$; that is, an increase in α of 0.36λ compared to infinite conjugate imaging.

4. Conclusions

Modern optical design involves a multi-parameter optimization for control of optical aberrations within the design envelop for the lens. The inclusion of digital signal processing and WFC within the design process for a SME zoom lens provides an additional set of tools that involves a trade-off of lens length and control of aberrations against SNR in the final image. We have shown how WFC enables an order-of-magnitude reduction in length of SME zoom lenses which, when combined with the benefits of recent reductions in detector dimensions, enables these lenses to be three orders-of-magnitude shorter than was possible using traditional 35 mm film technology. We have described a first-order design process that agrees with a ray-traced analysis. This is illustrated for a zoom lens with a 2.3x zoom factor and a length of only 10 mm. This reduction in lens length combined with relative simplicity of the lens has not previously been possible.

Acknowledgment

We would like to thank STMicroelectronics and Scottish Enterprise for funding.